Hindawi Publishing Corporation
Journal of Nanomaterials
Volume 2014, Article ID 708719, 9 pages
http://dx.doi.org/10.1155/2014/708719

Hindawi

Research Article

Influence of Impurities on the Luminescence of Er^{3+} Doped $BaTiO_3$ Nanophosphors

G. D. Webler,[1] M. J. M. Zapata,[1] G. S. Maciel,[2] A. Patra,[3] J. M. Hickmann,[1,4] and M. A. R. C. Alencar[1,5]

[1] *Optics and Materials Group (OPTMA), Universidade Federal de Alagoas, CP 2051, 57061-970 Maceió, AL, Brazil*
[2] *Instituto de Física, Universidade Federal Fluminense, 24210-346 Niterói, RJ, Brazil*
[3] *Department of Materials Science, Indian Association for the Cultivation of Science, Kolkata 700032, India*
[4] *Instituto de Física, Universidade Federal do Rio Grande do Sul, 91501-970 Porto Alegre, RS, Brazil*
[5] *Departamento de Fisica, Universidade Federal de Sergipe, Cidade Universitária Professor José Aloísio de Campos, Rodovia Marechal Rondon, s/n, Jardim Rosa Elze, 57072-970 São Cristóvão, SE, Brazil*

Correspondence should be addressed to M. A. R. C. Alencar; marca@optma.org

Received 6 December 2013; Revised 13 March 2014; Accepted 25 March 2014; Published 24 April 2014

Academic Editor: Edward A. Payzant

The influence of the presence of barium carbonate ($BaCO_3$) phase on the luminescence properties of barium titanate nanocrystals ($BaTiO_3$) powders was investigated. Structural and optical characterizations of erbium (Er^{3+}) doped $BaTiO_3$ synthesized by the sol-emulsion-gel were performed. Using Fourier transform infrared spectroscopy and X-ray powder diffraction, we identified the presence of impurities related to $BaCO_3$ and quantified its fraction. It was observed that the presence of $BaCO_3$ phase, even at low levels, depletes significantly the infrared-to-visible upconverted luminescence efficiency of the produced nanopowders.

1. Introduction

Nowadays there is a great interest in the development of materials with nanometric dimensions that can convert efficiently energy into light. Such interest arises from the intrinsic emission properties that these nanophosphors may exhibit related to their size, as well as the huge potential of applications which can be designed based on them, for instance, bioimaging systems [1–9] and sensors [10–17]. Different kinds of materials can be exploited as nanophosphors. However inorganic luminescent systems, for instance rare earth doped nanoparticles (REDN), have attracted a lot of interest owing to the advantages they possess in comparison with organic luminophores, such as low toxicity, superior photostability, and frequency upconversion emission.

Several works have been performed in recent years probing which physical parameters could influence the upconversion luminescence of REDN, as the optimization of such phenomena is essential for the development of more efficient nanophosphors. Up to this moment, it was observed that particle's size [10, 11, 18–32], shape [32], crystalline structure [21, 22, 28, 33], rare earth ion concentration [21, 24, 28, 33, 34], surrounding environment [11, 35], and presence of impurities [34] could modify significantly the performance of different kinds of REDN.

Among the investigated REDN, it has been shown that rare earth doped barium titanate ($BaTiO_3$) nanocrystals present many desirable properties for luminescent applications in nanoscale, such as low phonon energy, $\approx 540\,cm^{-1}$ [36], and efficient frequency upconversion processes. Due to this fact, it was demonstrated that erbium doped $BaTiO_3$ nanocrystal is an efficient nanophosphor for temperature sensing [10, 11]. $BaTiO_3$ is a typical ABO_3 perovskite type material with a variety of crystal structure modifications. Depending on the transition temperature, $BaTiO_3$ has five kinds of crystal systems, that is, hexagonal, cubic, tetragonal, orthorhombic, and rhombohedral [37]. On the other hand, one of the main difficulties encountered during the fabrication of $BaTiO_3$ is the presence of impurities originating from

their synthesis. Barium carbonate ($BaCO_3$) is the most frequently occurring impurity and it can be formed during the synthesis of $BaTiO_3$ powder, whichever route is used [38]. It should be emphasized that by using heat [39] and/or chemical treatments [40, 41], it is possible to reduce the presence of $BaCO_3$ in $BaTiO_3$ nanopowders. However, these procedures are not perfect because they cannot eliminate entirely the presence of $BaCO_3$; in addition the chemical procedures may induce the formation of different contaminants [38] and the heat treatment also increases the size of the produced nanocrystals [21]. Therefore, for very small sized $BaTiO_3$ nanocrystals, the presence of $BaCO_3$ is still a technological difficulty for the production of efficient nanophosphor.

Many parameters that can influence the upconversion emission from $BaTiO_3$ have been investigated so far, rare earth concentration [21], size [10, 11, 18, 21], environment [11], and temperature [10, 11]. However, although it is known that the presence of carbonates can be deleterious for luminescence of REDN, a direct or indirect measurement of the real influence of $BaCO_3$ presence on the upconversion fluorescence of rare earth doped $BaTiO_3$ nanopowder has been not reported yet.

In this work, we investigated how the presence of $BaCO_3$ modifies the infrared-to-visible frequency upconversion of $BaTiO_3$ nanocrytals doped with erbium ions. We quantified the amount of $BaCO_3$ on two samples of powdered $BaTiO_3$ and observed a direct correlation between the impurity concentration and the samples fluorescence intensity.

2. Experimental

The $BaTiO_3$ nanocrystals were produced using the sol-emulsion-gel method [21]. First, we prepare TiO_2 sol from titanium isopropoxide $Ti(OiPr)_4$, acetylacetone, and propanol. In short, 11 mL of $Ti(OiPr)_4$ was added to 19 mL of propanol and stirred for 15 min. A mixture of 19 mL propanol and of 1.82 mL acetylacetone was prepared in another beaker. It was added to the first mixture of $Ti(OiPr)_4$ and propanol and stirred for another 30 min. At last, 18.76 mL of propanol and 1.29 mL of H_2O were added to the mixture and stirred for more 2 hrs. The produced TiO_2 sol was slowly added, under vigorous stirring at ambient temperature, to a solution of $Ba(Ac)_2$ dissolved in water and acetic acid. Then, 2 mol% of erbium acetate was added to this sol. Cyclohexane and sorbitan monooleate (Span 80, fluka) were used as the organic liquid (oil phase) and the nonionic surfactant, respectively, in order to obtain emulsified droplets through water-in-oil type emulsions. The Er doped $BaTiO_3$ sol was then dispersed in the solvent under stirring condition. The sol droplets formed in the process were then gelled by controlled addition of a base. The gel particles were separated by centrifugation followed by washing with acetone and methanol. The product obtained was dried at 60°C for 12 hrs. The dried materials were heated at a rate of 2°/min and kept for 30 min at 700°C, for sample A, and 850°C for sample B. The powders were pressed to form thin disks with smooth surfaces and then cut to small pieces for optical measurements.

Transmission electron microscopy (TEM) images and energy dispersive X-ray spectroscopy were obtained using a FEI - Tecnai20 transmission electron microscope operating voltage at 200 kV, at the Centro de Tecnologias Estratégicas do Nordeste (CETENE). Samples for TEM were prepared by making a clear dispersion of the samples in acetone and placing a drop of the solution on a carbon coated copper grid. The solution was allowed to evaporate leaving behind the samples on the grid. An IR spectrometer (IRPrestige-21) equipped with diffuse reflectance accessory DRS8000 was used to identify the IR-active functional groups. A few milligrams of powder sample (2 mg) were mixed with a nonabsorbing standard (200 mg of potassium bromide, KBr) on a holder. Energy dispersive X-ray spectroscopy was also performed using a tabletop EDX equipment (EDX-800HS, Shimadzu). The crystalline phases of the particles were identified by X-ray powder diffraction (XRPD) using a Shimadzu model XRD-6000, powder X-ray diffractometer using a CuKα radiation (1.5418 Å), over the range 20 to 60 at a speed of 2 deg./min. The phases present in the sintered samples were identified by comparison of the diffraction patterns with the reference cards of the JCPDS powder diffraction file. The quantification of phases and the lattice parameters were determined using the Rietveld method [42] and the DBWSTools 2.3 software [43].

The optical measurements were carried out using mode-locked Ti:Sapphire laser, tuned at 800 nm, delivering 200 fs duration pulses with a 76 MHz repetition rate. The laser beam was focused on the surface of the nanocrystals' disks with normal incidence. The fluorescence was also collected normally to the disks' surface. The same lens was used to focus the incident beam and to collimate the luminescence. A cold mirror was employed to eliminate the laser scattered light and guide the fluorescence signal to an optical multimode fiber connected to a compact CCD spectrometer, Ocean Optics USB-4000. The measurements were carried out in such a way that the same laser intensity was employed and the intensity of the collected fluorescence was maximized for both samples.

3. Results and Discussion

In Figure 1, the FTIR spectra for the powders calcined at 700°C and 850°C are presented. As can be observed, both samples presented several peaks and bands associated to the symmetric and asymmetric stretching vibrations of water (3000–2800 cm^{-1}), a bicarbonate vibration (2450 cm^{-1}) [44], and the presence of CO_2 (2359 cm^{-1}). The other peaks can be associated to carbonates vibrations [38], the broad peak at ~1450 cm^{-1} that corresponds to the asymmetric stretch (1415 cm^{-1}) of the simple carbonate ion CO_3^{2-}, and to the unidentate carbonate ligand (asymmetric stretch, 1480 cm^{-1}, symmetric stretch, 1370 cm^{-1}), the peak at 1750 cm^{-1} related to an organic carbonate and peak at 1060 cm^{-1} [44]. These results demonstrated that there was a significant amount of barium carbonate within the produced $BaTiO_3$ powders. Unfortunately, due to the absence of suitable reference samples, it was not possible to quantify the amount of $BaCO_3$ in the investigated powders using this technique.

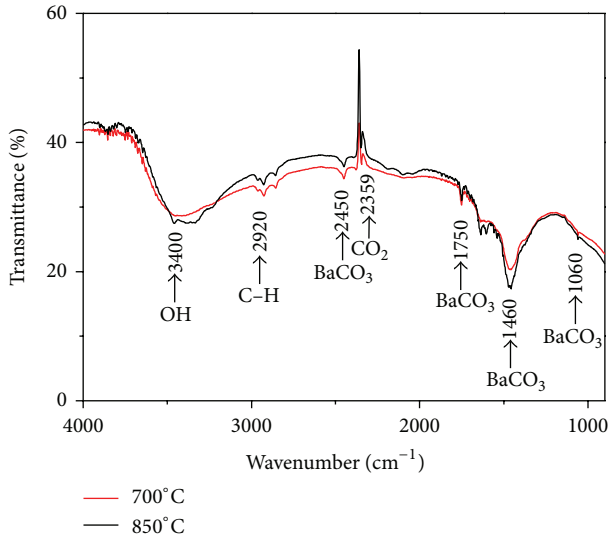

FIGURE 1: FTIR spectrum of $BaTiO_3 : Er^{3+}$ powders.

The size and the crystalline structure of the produced nanocrystals were characterized by TEM and XRDP measurements. In Figure 2, it is shown a typical TEM image of the nanopowders calcined at 700°C and 850°C. As can be observed, in both cases, two kinds of structure were present, small nanocrystals with average size around 25 nm and large rods.

Energy dispersive X-ray spectroscopy measurements were performed in order to identify if there was compositional difference between the two kinds of structures. The spectra obtained for crystals calcined at 700°C are presented in Figure 3. For small nanoparticles and large rods, the same components were identified: barium, titanium, erbium, carbon, copper, and oxygen. It must be emphasized that the cooper line can be attributed to the kind of the grid employed (SPI - 3620C-MB). However, the carbon signal might mean that there were some nanoparticles containing carbon atoms or that there was some contribution from the grid itself. Indeed, using the tabletop EDX, it was verified that copper signal is not present when there was no grid, while the carbon levels could not be detected due to this system limitations.

Nevertheless, some differences between the distinct nanostructures could be detected. First, the relative intensity of the erbium peak in comparison with the others elements was much smaller for the site with only rods. This suggests that the erbium ions concentration is higher in the smaller particles than in the rods. Second, the peak height related to the presence of carbon in comparison with the barium and titanium peaks is larger for the site with rods. This result indicates that the carbon concentration in the rod is also larger. At last, we could not identify if the increase of the carbon concentration for the measurements in rods was coupled with a titanium amount decrease, as there is an overlap of barium L-band and the titanium K-band.

In Figure 4, the typical XRPD pattern of both samples is presented. It can be observed that both powders present two phases, identified as a cubic structure of $BaTiO_3$ (PDF number 79-2263) and an orthorhombic structure of $BaCO_3$ (PDF number 71-2394). The crystal sizes of the $BaTiO_3$ phase nanocrystals were calculated using Scherrer's equation, applied to the diffraction line associated to the (110) plane. The calculated average crystal sizes were 22.9 nm for sample A and 26.8 nm for sample B.

Therefore the combination of the TEM, EDS, and XRPD suggests that the investigated samples appear to be consisting predominately of $BaTiO_3$ small particles and large rods of $BaCO_3$, which is a similar result as reported in [44].

Using the Rietveld refinement method, we could estimate the concentration of both crystalline phases in the powders calcined at the different temperatures. In Figure 5, the obtained refinement for the sample calcined at 700°C is presented. For this sample, we estimated a percentage of 90.18% and 9.82% for $BaTiO_3$ and $BaCO_3$ phases, respectively. The lattice parameters found for the first phase ($BaTiO_3$) are $a = b = c = 4.0129$ Å and phase 2 ($BaCO_3$) are $a = 5.2820$ Å, $b = 8.9596$ Å, and $c = 6.4368$ Å. As the TEM and EDS measurements indicated that the erbium ions were present in both kind of structures, but with a larger concentration in the small particles and assuming that the rods are consisted predominantly of $BaCO_3$ phase, while the $BaTiO_3$ phase is composed by the small particles, it was considered that the erbium ions could be present in both phases in the refinement calculations. Following this procedure, the best refinement results were obtained considering that the molar concentration of erbium ions in the $BaTiO_3$ and $BaCO_3$ phases was equal to 2.1% and 0.9% respectively.

The same approach was employed in the refinement for the powder calcined at 850°. The result is shown in Figure 6. For this sample, we obtained a percentage of 94.87% and 5.13% for phases of $BaTiO_3$ and $BaCO_3$, respectively. The lattice parameters found for the first phase ($BaTiO_3$) are $a = b = c = 4.0128$ Å and phase 2 ($BaCO_3$) are $a = 5.2835$ Å, $b = 9.0057$ Å, and $c = 6.4433$ Å. In this case, it was obtained that the molar concentration of erbium ions were equal to 2.2% in the $BaTiO_3$ phase and 0.4% in the $BaCO_3$ phase.

It should be noticed that the obtained values for erbium ions' molar concentrations in barium carbonate phase are just an approximation. Due to the low concentration of $BaCO_3$, the uncertainties of these estimated quantities can be very high. Moreover, other effects such as surface strains might play an important role to the changes of the lattice parameters. However, owing to the other characterization techniques results, the assumption that erbium ions are present in both phases seems to be suitable for the investigated samples.

The fluorescence spectroscopy results are presented in Figure 7. As can be observed, both samples presented intense infrared-to-green and infrared-to-red frequency upconversion. The physical mechanisms of these emissions have been discussed in detail in previous works [10, 11, 18, 21] and are related to an excited state absorption process involving two laser photons and it is represented schematically in Figure 8. Briefly, a first laser photon is absorbed promoting a transition from the ground state $^4I_{15/2}$ to the $^4I_{9/2}$ excited state of the erbium ion. Then, the ion decays nonradiatively to the $^4I_{11/2}$ or $^4I_{13/2}$. A second absorption step may occur from these two

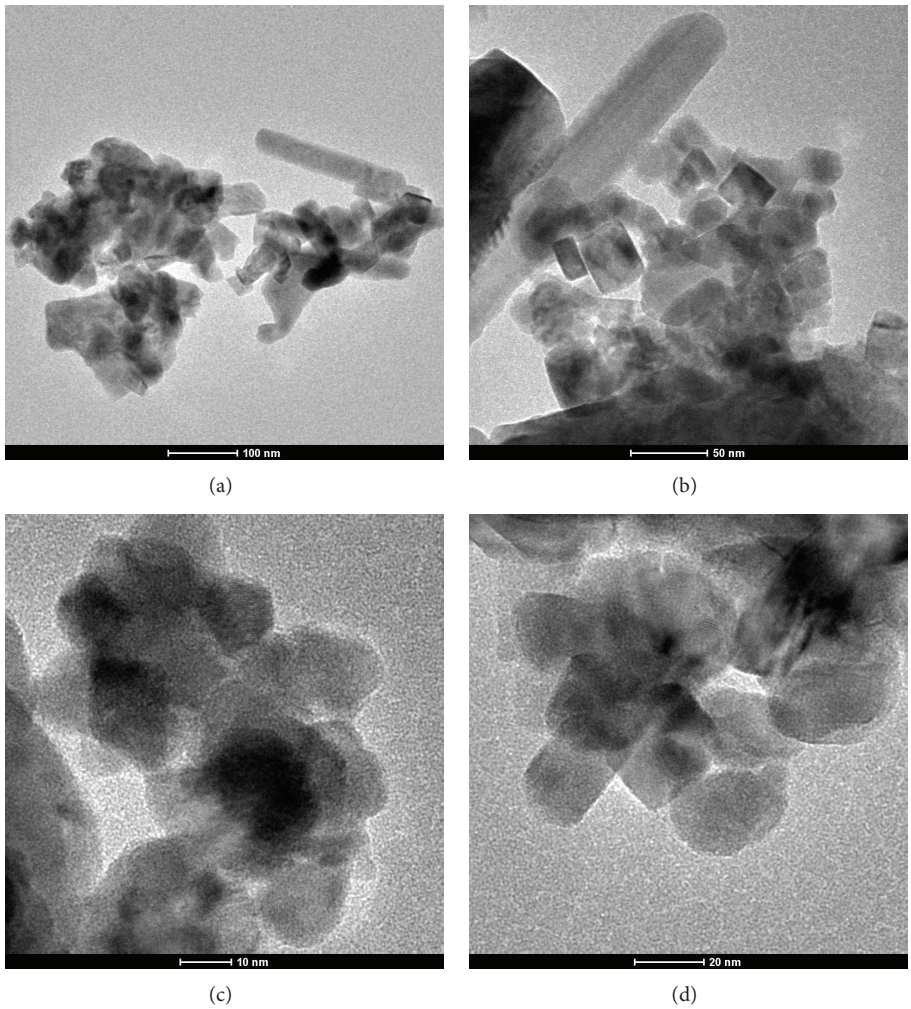

Figure 2: TEM images of the investigated nanopowders displaying the different particles shape and size for the crystals calcined at (a) 700°C and (b) 850°C. Detailed views of the $BaTiO_3$ nanocrystals calcined at (c) 700°C and (d) 850°C are also shown.

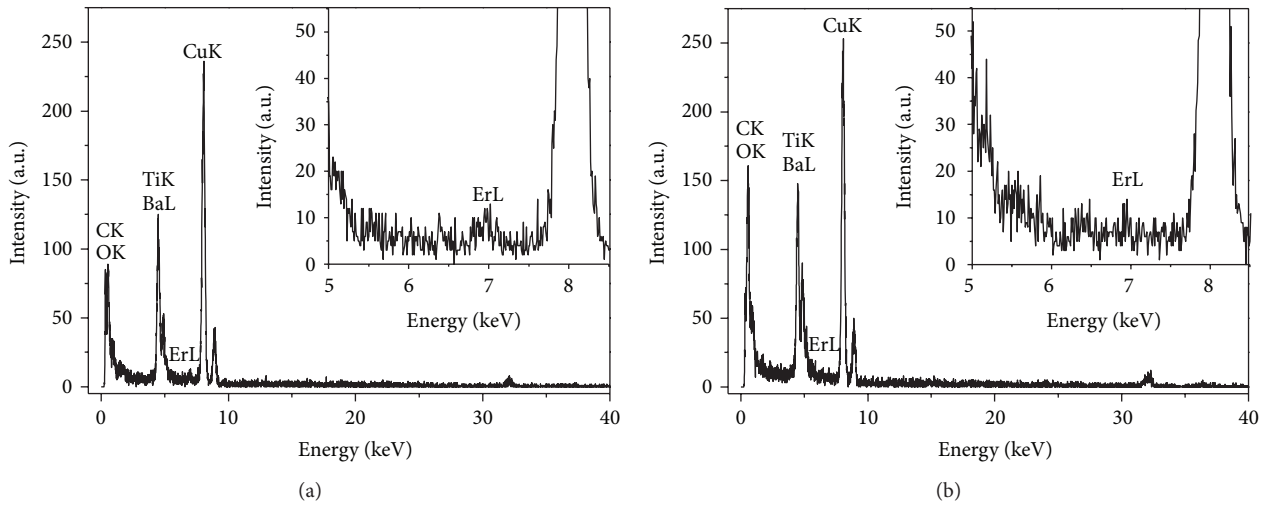

Figure 3: EDS spectra of crystals calcined at 700°C, measured for samples containing only (a) small particles and (b) large rods.

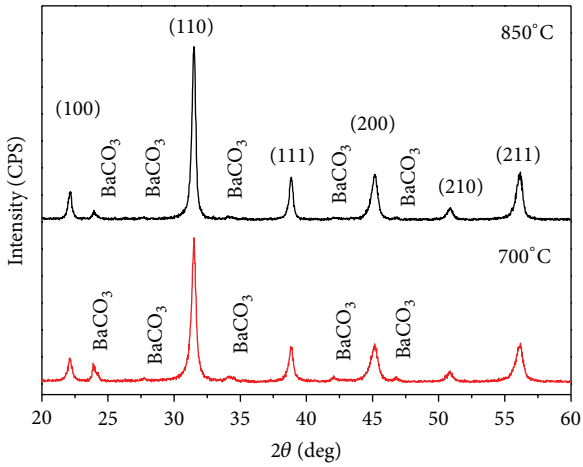

FIGURE 4: X-ray diffraction pattern of 2 mol% Er doped $BaTiO_3$ nanocrystals calcined at 700°C and 850°C.

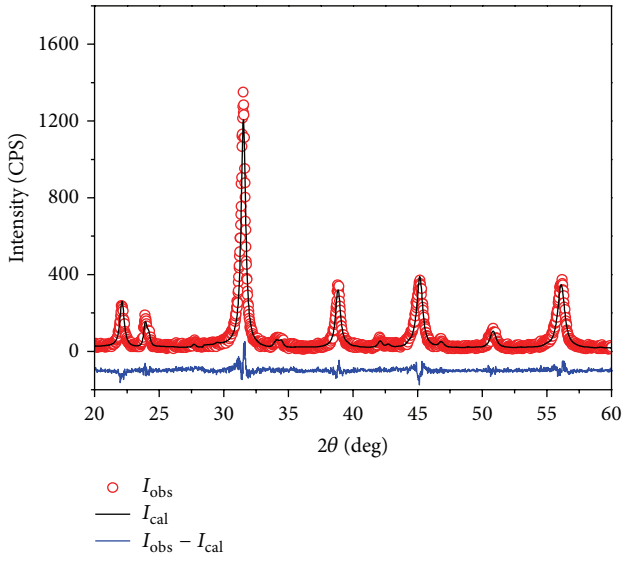

FIGURE 5: The structural refinement patterns of $BaTiO_3$ (sample A) using X-ray powder diffraction data. Open red circles correspond to the experimental data (I_{obs}); solid black line is the calculated pattern (I_{cal}), while the blue line is the difference between the experimental and the theoretical curves. In this refinement, the coefficients of reliability were $R_e = 13.21\%$, $R_{wp} = 16.25\%$, and $S = R_e/R_{wp} = 1.23$.

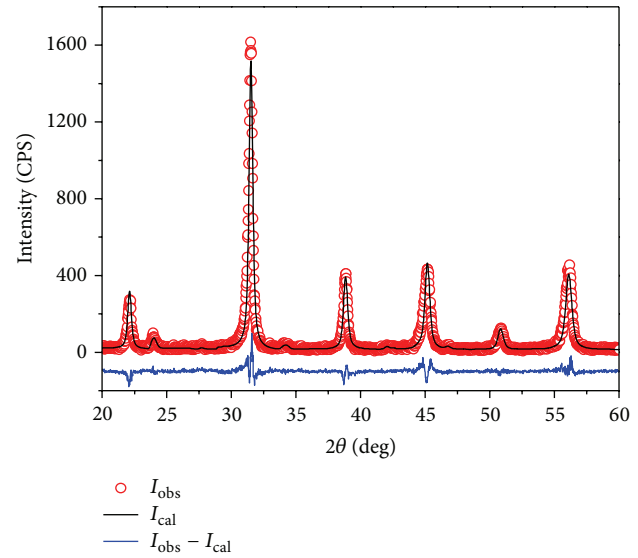

FIGURE 6: The structural refinement patterns of $BaTiO_3$ (sample B) using X-ray powder diffraction data. Open red circles correspond to the experimental data (I_{obs}); solid black line is the calculated pattern (I_{cal}), while the blue line is the difference between the experimental and theoretical curves. In this case, $R_e = 13.79\%$, $R_{wp} = 18.19\%$, and $S = 1.32$.

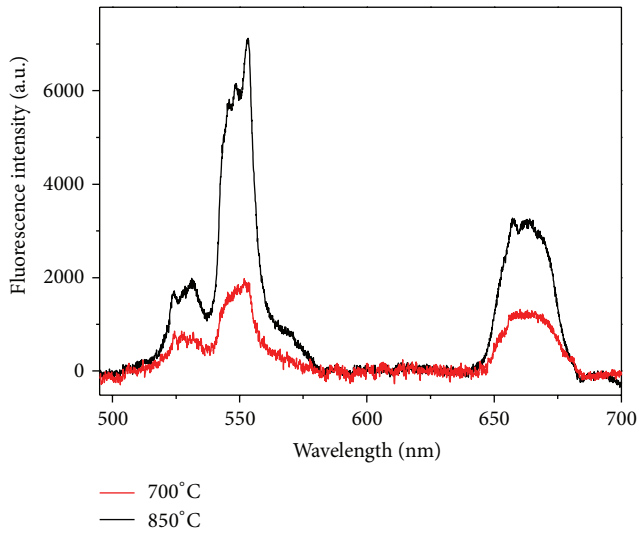

FIGURE 7: Upconverted luminescence from samples A and B for excitation laser tuned at 800 nm and 260 mW average power.

levels populating the excited state $^4F_{3/2}$ or populating directly the fluorescent levels $^2H_{11/2}$and $^4S_{3/2}$. Population at level $^4F_{3/2}$ may also decay nonradiatively to fluorescent levels $^2H_{11/2}$and $^4S_{3/2}$. The $^4F_{9/2}$ level is populated nonradiatively from higher energy levels. Finally, radiative transitions $^2H_{11/2} \rightarrow {}^4I_{15/2}$, $^2S_{3/2} \rightarrow {}^4I_{15/2}$, and $^4F_{9/2} \rightarrow {}^4I_{15/2}$ occur, generating the observed fluorescence bands centered at 530 nm, 550 nm, and 660 nm, respectively.

As can be seen in Figure 7, although both samples present the same erbium concentration, nanoenvironment, $BaTiO_3$ crystalline structure, and comparable nanocrystals average size, there is a huge difference on the emitted fluorescence. Indeed, the sample B has a stronger upconversion luminescence when compared with the sample A. As the measurements were carried out with the powders within the same environment, erbium concentration, and temperature, the size and the impurities concentration differences between the powders give the most important contribution to the observed distinct fluorescence intensities.

In order to evaluate the individual contribution of each these factors we compare our results with others reported

Table 1: Summary of the fitting parameters for the fluorescence of three different erbium-doped nanocrystals and ratio between the fluorescence integrated intensity for crystals with 26.8 nm and 22.9 nm diameter calculated using (1).

Nanocrystals	I_0	D (nm)	C	$I(26.8)/I(22.9)$
$BaTiO_3:Er^{3+}$ [18]	$(1.2 \pm 0.1) \times 10^{-3}$	15.5 ± 0.4	-0.8 ± 0.1	1.24
$BaYF_5:Yb^{3+}/Er^{3+}$ [19]	290 ± 20	18 ± 1	-0.8 ± 0.1	1.20
$Y_2O_3:Er^{3+}$ [20]	$(11 \pm 4) \times 10^3$	20 ± 1	-0.8 ± 0.1	1.17

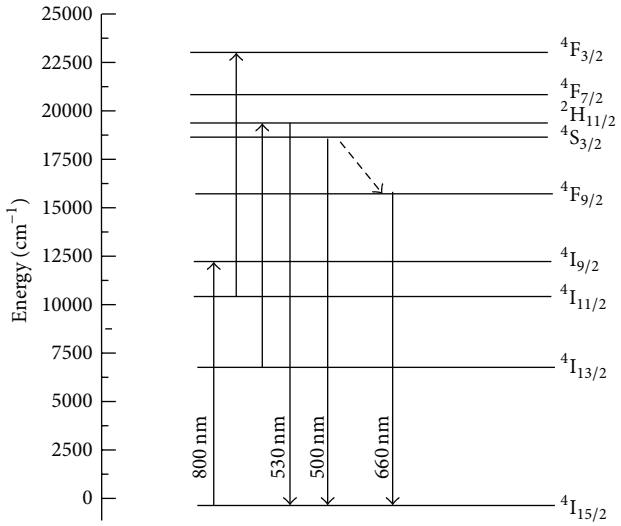

Figure 8: Simplified Er^{3+} energy levels scheme and frequency upconversion pathways.

in the literature. The size effect over the upconversion fluorescence intensity of nanophosphors has been investigated by different groups and distinct rare-earth doped materials. It has been observed that, in the range of 10 to 100 nm diameter nanocrystals, the luminescence is increased as the particles size is raised. For $BaTiO_3$ nanopowders in particular, it was possible to estimate empirically the behavior of the upconverted luminescence intensity as a function of the particles diameter, based on the results of a previous work [18]. In Figure 9 a graph of the integrated fluorescence intensity is plotted, including only the green and red upconverted emission as a function of the nanocrystals average diameter. This plot showed that the integrated fluorescence intensity increased nonlinearly with the crystals sizes. We observed that the best fitting results were achieved when we employed a single exponential expression to relate the luminescence intensity (I) and the crystal diameter (d):

$$I(d) = I_0\left(e^{d/D} + C\right), \quad (1)$$

where I_0, D, and C are fitting parameters. We performed the same procedure using the results of other pure erbium doped and ytterbium-erbium codoped nanocrystalline systems [19, 20] and obtained exponential fits, with similar values for constants D and C. A summary of these fitting factors are presented in Table 1. This result suggests that it is possible to obtain a factor that relates the relative change of the fluorescence intensity of erbium doped nanocrystals of different sizes.

Employing the results displayed in Table 1, we estimated that fluorescence of erbium doped nanocrystals with 26.8 nm should be roughly 1.20 ± 0.03 times larger than the luminescence of 22.9 nm nanocrystals in average. However, our experimental results showed that the fluorescence emitted by the sample calcined at 850°C is actually about 2.63 times greater than that emitted by the sample to 700°C, which clearly indicates that the size difference cannot explain the observed behavior and the presence of impurities must play an important role on the nanophosphors fluorescence.

We also calculated the ratio of the integrated intensities for the red and the green emission bands obtained for the samples A and B. Our results show that this ratio is 1.25 times larger for the sample A. As the erbium concentration and the environment are the same, this difference can be attributed only to the increase of the nonradiative transition rates on the sample with the largest $BaCO_3$ concentration. Indeed, as the phonon energies of $BaCO_3$ are larger than $BaTiO_3$ crystals, its presence gives a strong contribution to the depletion of the fluorescence intensity because of a combination of two mechanisms. The first one is related to the increase of new nonradiative transition paths that the Er^{3+} ions on the surface of $BaTiO_3$ nanocrystals experience provided by the presence of $BaCO_3$ in the neighborhood. It happens because the fluorescence from rare-earth ions present at the surface is influenced by nonradiative relaxation channels (defects at the surface of nanoparticle) that are not only related to the lattice vibrational modes of its host but also to high-energy modes of residual carbonates (1500 cm^{-1}) and hydroxyl ions (3350 cm^{-1}) adsorbed in the crystallite surfaces [21]. The second is associated to the excitation of the Er^{3+} ions that are currently doping the $BaCO_3$ phase. As this erbium doped material presents very poor fluorescence efficiency, the emission from the sample with larger relative amount of $BaCO_3$ must be smaller. Moreover, it was observed that the $BaCO_3$ concentration on the sample A is 2.43 times larger than sample B and the powder with the largest amount of impurities (sample A) presented lower luminescence intensity. This quantitative evidence indicates that fluorescence intensity is strongly correlated to the impurities concentration, even for small amounts.

4. Conclusion

In summary, we analyzed the upconversion luminescence properties of Er^{3+} doped $BaTiO_3$ nanocrystals prepared by

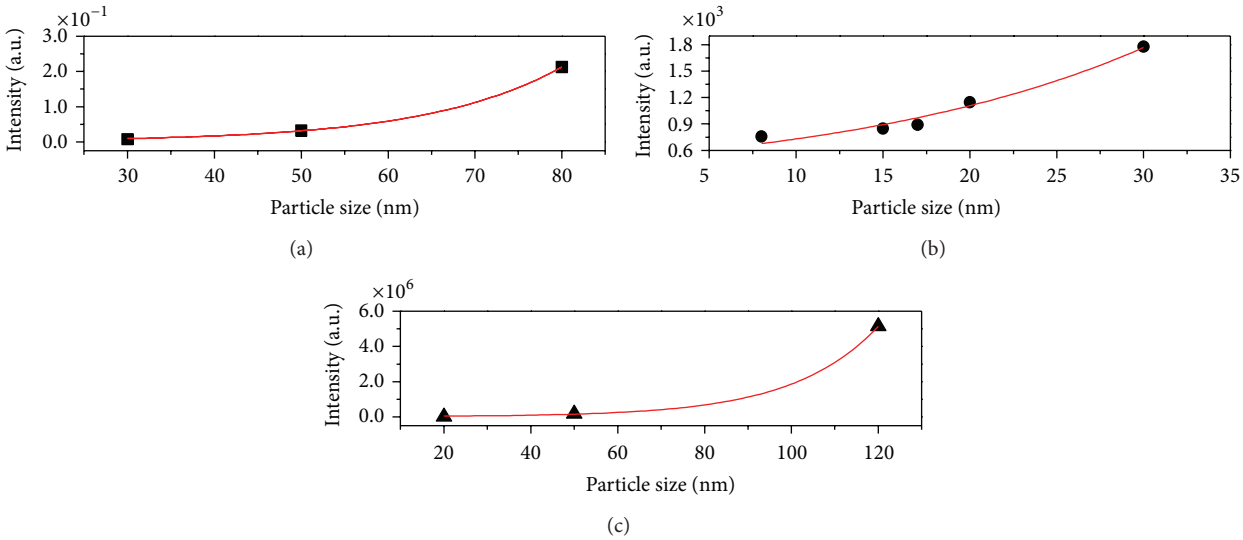

FIGURE 9: Integrated fluorescence intensity, including only the green and red upconverted emission as a function of the nanocrystals average diameter for (a) $BaTiO_3 : Er^{3+}$ [18], (b) $BaYF_5 : Yb^{3+}/Er^{3+}$ [19], and (c) $Y_2O_3 : Er^{3+}$ [20].

sol-emulsion-gel method and prepared at different temperatures. The heat-treatment process yielded samples with different particle sizes and $BaCO_3$ concentration. We observed a huge difference on the fluorescence intensity exhibited by both samples that can be attributed mainly to the change in the impurity concentrations of these powders. Our results demonstrate that, even at very low concentration, the presence of impurities may modify significantly the luminescence of erbium doped $BaTiO_3$ nanocrystals.

Conflict of Interests

The authors declare that there is no conflict of interests regarding the publication of this paper.

Acknowledgments

The authors thank the financial support from CAPES Pró-equipamentos/PROCAD/PROCAD-NF, CNPq/MCT, Pronex/FAPEAL, PADCT, Nanofoton Network, Instituto Nacional de Ciência e Tecnologia Fotônica para Telecomunicações, and FINEP. The authors also thank the Centro de Tecnologias Estratégicas do Nordeste (CETENE) for the transmission electron microscopy images employed in this work.

References

[1] Q. Q. Zhan, J. Qian, H. Liang et al., "Using 915 nm laser excited $Tm^{3+}/Er^{3+}/Ho^{3+}$-doped NaYbF4 upconversion nanoparticles for *in vitro* and deeper *in vivo* bioimaging without overheating irradiation," *ACS Nano*, vol. 5, no. 5, pp. 3744–3757, 2011.

[2] X.-F. Yu, Z. Sun, M. Li et al., "Neurotoxin-conjugated upconversion nanoprobes for direct visualization of tumors under near-infrared irradiation," *Biomaterials*, vol. 31, no. 33, pp. 8724–8731, 2010.

[3] L.-Q. Xiong, Z.-G. Chen, M.-X. Yu, F.-Y. Li, C. Liu, and C.-H. Huang, "Synthesis, characterization, and *in vivo* targeted imaging of amine-functionalized rare-earth up-converting nanophosphors," *Biomaterials*, vol. 30, no. 29, pp. 5592–5600, 2009.

[4] F. Wang, D. Banerjee, Y. Liu, X. Chen, and X. Liu, "Upconversion nanoparticles in biological labeling, imaging, and therapy," *Analyst*, vol. 135, no. 8, pp. 1839–1854, 2010.

[5] C. Wang, L. A. Cheng, and Z. A. Liu, "Drug delivery with upconversion nanoparticles for multi-functional targeted cancer cell imaging and therapy," *Biomaterials*, vol. 32, no. 4, pp. 1110–1120, 2011.

[6] R. Kumar, M. Nyk, T. Y. Ohulchanskyy, C. A. Flask, and P. N. Prasad, "Combined optical and MR bioimaging using rare earth ion doped $NaYF_4$ nanocrystals," *Advanced Functional Materials*, vol. 19, no. 6, pp. 853–859, 2009.

[7] B. A. Dong, S. Xu, J. Sun et al., "Multifunctional $NaYF_4$:Yb^{3+}, Er^{3+}@Ag core/shell nanocomposites: integration of upconversion imaging and photothermal therapy," *Journal of Materials Chemistry*, vol. 21, no. 17, pp. 6193–6200, 2011.

[8] Z. G. Chen, L. Zhang, Y. Sun, J. Hu, and D. Wang, "980-nm laser-driven photovoltaic cells based on rare-earth up-converting phosphors for biomedical applications," *Advanced Functional Materials*, vol. 19, no. 23, pp. 3815–3820, 2009.

[9] M. Nyk, R. Kumar, T. Y. Ohulchanskyy, E. J. Bergey, and P. N. Prasad, "High contrast *in vitro* and *in vivo* photoluminescence bioimaging using near infrared to near infrared up-conversion in Tm^{3+} and Yb^{3+} doped fluoride nanophosphors," *Nano Letters*, vol. 8, no. 11, pp. 3834–3838, 2008.

[10] M. A. R. C. Alencar, G. S. Maciel, C. B. de Araújo, and A. Patra, "Er^{3+}-doped $BaTiO_3$ nanocrystals for thermometry: influence of nanoenvironment on the sensitivity of a fluorescence based temperature sensor," *Applied Physics Letters*, vol. 84, no. 23, pp. 4753–4755, 2004.

[11] A. Patra, G. S. Maciel, M. A. R. C. Alencar, and C. B. de Araújo, "Upconversion emission of $BaTiO_3$:Er^{3+} nanocrystals: influence of temperature and surrounding medium," *Journal of*

Nanoscience and Nanotechnology, vol. 10, no. 3, pp. 2143–2148, 2010.

[12] L. N. Sun, H. Peng, M. I. J. Stich, D. Achatz, and O. S. Wolfbeis, "pH sensor based on upconverting luminescent lanthanide nanorods," *Chemical Communications*, no. 33, pp. 5000–5002, 2009.

[13] F. Vetrone, R. Naccache, A. Zamarrón et al., "Temperature sensing using fluorescent nanothermometers," *ACS Nano*, vol. 4, no. 6, pp. 3254–3258, 2010.

[14] E. Botzung-Appert, V. Monnier, T. H. Duong, R. Pansu, and A. Ibanez, "Polyaromatic luminescent nanocrystals for chemical and biological sensors," *Chemistry of Materials*, vol. 16, no. 9, pp. 1609–1611, 2004.

[15] V. Monnier, E. Dubuisson, N. Sanz-Menez et al., "Selective chemical sensors based on fluorescent organic nanocrystals confined in sol–gel coatings of controlled porosity," *Microporous and Mesoporous Materials*, vol. 132, no. 3, pp. 531–537, 2010.

[16] A. G. Joshi, S. Sahai, N. Gandhi, Y. G. R. Krishna, and D. Haranath, "Valence band and core-level analysis of highly luminescent ZnO nanocrystals for designing ultrafast optical sensors," *Applied Physics Letters*, vol. 96, no. 12, Article ID 123102, 2010.

[17] A. S. Susha, A. M. Javier, W. J. Parak, and A. L. Rogach, "Luminescent CdTe nanocrystals as ion probes and pH sensors in aqueous solutions," *Colloids and Surfaces A: Physicochemical and Engineering Aspects*, vol. 281, no. 1–3, pp. 40–43, 2006.

[18] P. Ghosh, S. Sadhu, T. Sen, and A. Patra, "Upconversion emission of $BaTiO_3$: Er nanocrystals," *Bulletin of Materials Science*, vol. 31, no. 3, pp. 461–465, 2008.

[19] J. Y. Sun, J. Xian, X. Zhang, and H. Du, "Size and shape controllable synthesis of oil-dispersible $BaYF_5$:Yb^{3+}/Er^{3+} upconversion fluorescent nanocrystals," *Journal of Alloys and Compounds*, vol. 509, no. 5, pp. 2348–2354, 2011.

[20] S. G. Xiao and X. L. Yang, "Size-dependent upconversion properties of Er^{3+} doped nano Y_2O_3 particles," *Modern Physics Letters B*, vol. 25, no. 4, pp. 265–272, 2011.

[21] P. N. Prasad, A. Patra, C. S. Friend, and R. Kapoor, "Fluorescence upconversion properties of Er^{3+}-doped TiO_2 and $BaTiO_3$ nanocrystallites," *Chemistry of Materials*, vol. 15, no. 19, pp. 3650–3655, 2003.

[22] G. S. Maciel and A. Patra, "Influence of nanoenvironment on luminescence lifetime of Er^{3+}-activated ZrO_2 nanocrystals," *Journal of the Optical Society of America B: Optical Physics*, vol. 21, no. 3, pp. 681–684, 2004.

[23] X. Bai, H. Song, G. Pan et al., "Size-dependent upconversion luminescence in Er^{3+}/Yb^{3+}-COdOpCd nanocrystalline yttria: saturation and thermal effects," *The Journal of Physical Chemistry C*, vol. 111, no. 36, pp. 13611–13617, 2007.

[24] G. Y. Chen, T. Y. Ohulchanskyy, R. Kumar, H. Ågren, and P. N. Prasad, "Ultrasmall monodisperse $NaYF_4$:Yb^{3+}/Tm^{3+} nanocrystals with enhanced near-infrared to near-infrared upconversion photoluminescence," *ACS Nano*, vol. 4, no. 6, pp. 3163–3168, 2010.

[25] C. H. Liu, J. Sun, H. Wang, and D. Chen, "Size and morphology controllable synthesis of oil-dispersible LaF_3:Yb,Er upconversion fluorescent nanocrystals via a solid-liquid two-phase approach," *Scripta Materialia*, vol. 58, no. 2, pp. 89–92, 2008.

[26] Y. X. Liu, C. F. Xu, and Q. B. Yang, "White upconversion of rare-earth doped ZnO nanocrystals and its dependence on size of crystal particles and content of Yb^{3+} and Tm^{3+}," *Journal of Applied Physics*, vol. 105, no. 8, Article ID 084701, 2009.

[27] H.-X. Mai, Y.-W. Zhang, L.-D. Sun, and C.-H. Yan, "Size- and phase-controlled synthesis of monodisperse $NaYF_4$:Yb,Er nanocrystals from a unique delayed nucleation pathway monitored with upconversion spectroscopy," *The Journal of Physical Chemistry C*, vol. 111, no. 37, pp. 13730–13739, 2007.

[28] A. M. Pires, S. Heer, H. U. Güdel, and O. A. Serra, "Er, Yb doped yttrium based nanosized phosphors: particle size, "host lattice" and doping ion concentration effects on upconversion efficiency," *Journal of Fluorescence*, vol. 16, no. 3, pp. 461–468, 2006.

[29] S. Schietinger, L. D. S. Menezes, B. Lauritzen, and O. Benson, "Observation of size dependence in multicolor upconversion in single Yb^{3+}, Er^{3+} codoped $NaYF_4$ nanocrystals," *Nano Letters*, vol. 9, no. 6, pp. 2477–2481, 2009.

[30] F. Shi, J. Wang, D. Zhang, G. Qin, and W. Qin, "Greatly enhanced size-tunable ultraviolet upconversion luminescence of monodisperse β-$NaYF_4$:Yb,Tm nanocrystals," *Journal of Materials Chemistry*, vol. 21, no. 35, pp. 13413–13421, 2011.

[31] J. Silver, M. I. Martinez-Rubio, T. G. Ireland, G. R. Fern, and R. Withnall, "The effect of particle morphology and crystallite size on the upconversion luminescence properties of erbium and ytterbium co-doped yttrium oxide phosphors," *The Journal of Physical Chemistry B*, vol. 105, no. 5, pp. 948–953, 2001.

[32] J. N. Shan, M. Uddi, R. Wei, N. Yao, and Y. Ju, "The hidden effects of particle shape and criteria for evaluating the upconversion luminescence of the lanthanide doped nanophosphors," *The Journal of Physical Chemistry C*, vol. 114, no. 6, pp. 2452–2461, 2010.

[33] A. Patra, "Effect of crystal structure and concentration on luminescence in Er^{3+}:ZrO_2 nanocrystals," *Chemical Physics Letters*, vol. 387, no. 1–3, pp. 35–39, 2004.

[34] J. A. Capobianco, F. Vetrone, J. C. Boyer, A. Speghini, and M. Bettinelli, "Enhancement of red emission ($^4F_{9/2} \rightarrow {}^4I_{15/2}$) via upconversion in bulk and nanocrystalline cubic Y_2O_3:Er^{3+}," *The Journal of Physical Chemistry B*, vol. 106, no. 6, pp. 1181–1187, 2002.

[35] R. S. Meltzer, S. P. Feofilov, B. Tissue, and H. B. Yuan, "Dependence of fluorescence lifetimes of Y_2O_3:Eu^{3+} nanoparticles on the surrounding medium," *Physical Review B: Condensed Matter and Materials Physics*, vol. 60, no. 20, pp. R14012–R14015, 1999.

[36] X. Q. Jin, D. Sun, M. Zhang, Y. Zhu, and J. Qian, "Investigation on FTIR spectra of barium calcium titanate ceramics," *Journal of Electroceramics*, vol. 22, no. 1–3, pp. 285–290, 2009.

[37] C. J. Xiao, C. Q. Jin, and X. H. Wang, "Crystal structure of dense nanocrystalline $BaTiO_3$ ceramics," *Materials Chemistry and Physics*, vol. 111, no. 2-3, pp. 209–212, 2008.

[38] M. D. B. Lopez, G. Fourlaris, B. Rand, and F. L. Riley, "Characterization of barium titanate powders: barium carbonate identification," *Journal of the American Ceramic Society*, vol. 82, no. 7, pp. 1777–1786, 1999.

[39] M. Stockenhuber, H. Mayer, and J. A. Lercher, "Preparation of barium titanates from oxalates," *Journal of the American Ceramic Society*, vol. 76, no. 5, pp. 1185–1190, 1993.

[40] C. Herard, A. Faivre, and J. Lemaitre, "Surface decontamination treatments of undoped $BaTiO_3$—part II: influence on sintering," *Journal of the European Ceramic Society*, vol. 15, no. 2, pp. 145–153, 1995.

[41] C. Herard, A. Faivre, and J. Lemaitre, "Surface decontamination treatments of undoped $BaTiO_3$—part I: powder and green body properties," *Journal of the European Ceramic Society*, vol. 15, no. 2, pp. 135–143, 1995.

[42] D. B. Wiles and R. A. Young, "A new computer program for Rietveld analysis of X-ray powder diffraction patterns," *Journal of Applied Crystallography*, vol. 14, part 2, pp. 149–151, 1981.

[43] L. Bleicher, J. M. Sasaki, and C. O. P. Santos, "Development of a graphical interface for the Rietveld refinement program *DBWS*," *Journal of Applied Crystallography*, vol. 33, part 4, p. 1189, 2000.

[44] S. L. M. Brito and D. Gouvêa, "Surface characterization of $BaTiO_3$ nanoparticles prepared by the polymeric precursor method," *Cerâmica*, vol. 56, no. 339, pp. 228–236, 2010.